Progress In Electromagnetics Research B, Vol. 20, 167–186, 2010

ANALYTICAL MODELING OF THE PRINTED DIPOLE ANTENNA LOADED WITH CRLH STRUCTURES

M. Rafaei Booket, M. Kamyab, A. Jafargholi and S. M. Mousavi

Department of Electrical Engineering
K. N. Toosi University of Technology (KNTU)
Tehran, Iran

Abstract—In this paper, an analytical method to characterize the frequency behaviour of Composite Right/Left Handed (CRLH) loaded printed dipole antenna is presented. One needs to determine the parameters of ungrounded reactive components realizing CRLH structures. Efficient resonant RLC circuit models based on Partial Elements Theory are presented to calculate inductance of meander line inductor and inter digital capacitor, while their capacitance is determined by Conformal Mapping Method. By using these circuit models and dispersion relation of balanced CRLH TL, negative resonance modes of antenna can be obtained. In addition, to validate the accuracy of the proposed analytical method, a prototype of the CRLH loaded printed dipole antenna is simulated, fabricated and measured.

1. INTRODUCTION

In recent years, a novel kind of artificial structures known as Composite Right-Left Handed (CRLH) structures has become subject of growing interest in antenna engineering because of their left-handed properties, not found in nature. Usually constructed by small, compared to the wavelength, components arranged in periodic manner. The transmission lines loaded with reactive components having left-handed behaviour have been applied to many forms of antennas such as dipoles and loops, to improve their performance. Left-Hand concepts have been used to microstrip transmission lines [1], and microwave circuits [2]. In [3] high pass filters have been designed by using of balanced CRLH/CSRR-based metamaterial transmission lines. In [4]

Corresponding author: M. Rafaei Booket (m.rafaeibookat@ee.kntu.ac.ir).

a CRLH microstrip delay line, which simultaneously exhibits negative refractive index and negative group-delay, has been presented. CRLH and Extended CRLH (ECRLH) transmission lines have been studied and evaluated to find the most suitable structure for dual band power amplifiers in [5]. In [6] a leaky wave antenna consisting of microstrip transmission lines has been presented. The left-handed TL concept has been also applied to small antennas constructed on a ground plane [7, 8]. Applications such as an infinitesimal dipole immersed in left-handed material [9], the left-handed ladder network to form a small dipole antenna [10], a short dipole antenna and an orthogonally polarized dipole antenna have been studied in [11]. Loading CRLH structures has been successfully applied to antennas to achieve an equivalently miniaturized design. Some simulations have been also presented for enhancement the efficiency of the left-hand loaded dipole antennas in [12]. However, analytical modeling and governing formula versus CRLH parameters for investigating the frequency behaviour and design of the printed dipole antennas loaded with CRLH structures has not yet been presented.

In [13] rectangular shape complementary split ring resonators (CSRRs) with different dimensions are introduced to realize balanced Composite Right/Left Handed (CRLH) structure and their propagation characteristics are demonstrated. A novel artificial transmission line with Left/Right Handed behavior based on wire bonded inter digital capacitors provided a wider frequency band of operation has been presented in [14]. In this paper, the CRLH structures is comprised by repetition of inter digital capacitors as series and meander line inductors as shunt components into a host conventional TL exhibiting a LH band at lower frequencies and a RH band at higher frequencies. Analysis of the CRLH loaded dipole antenna is presented based on the dispersion relation of an infinite CRLH TL [15]. In this case, the CRLH structures do not include a ground plane, capacitance and inductance of ungrounded inter digital capacitors and ungrounded meander line inductors should be calculated versus physical layout parameters for antenna frequency behavior analysis.

A partial-element equivalent circuit model (PEEC) for the inductance determination of grounded meander line inductors printed on circuit boards and their capacitance determination by means of curve fitting has been presented in [16], while, parameters determination of ungrounded meander line inductors has not yet been presented. Also, more accurate calculation for inter digital capacitance is obtained by analytical formulation reported in [17], but inductance determination of them has not yet been presented.

In this paper, novel formulas for calculating the parameters of ungrounded reactive components forming CRLH structures are presented. In other words, inductance and capacitance of ungrounded meander line and inter digital structures are determined analytically using quasi-static approximation. The results of which are in close agreement with those obtained through simulation and available measurement data. Also, comprised [11], this proposed antenna has superiority in miniaturization and bandwidth.

In this paper, inductance and capacitance calculations of ungrounded meander line and ungrounded inter digital structures are presented in next section. Analysing and design of proposed antenna is described in Section 3. The implementation of the CRLH dipole antenna is described in Section 4 with measurement and simulation results obtained by the High Frequency Structure Simulator (HFSS).

2. ANALYTICAL MODELING OF MEANDERLINE INDUCTOR AND INTERDIGITAL CAPACITOR

2.1. Ungrounded Meander Line Inductor

As stated earlier, printed ungrounded meander line inductor can be used as the shunt element in transmission line for realization of CRLH structures, Figure 1 shows a single turn of ungrounded meaner line inductor. The inductance of a grounded meander line has been calculated and presented along with measured data [16]. In this paper, first, we use quasi-static approximation to analytically determine the inductance of a meander line with ground plane and the results are compared with those reported in [16] in order to validate our proposed method, then our method is applied to cases with ground plane removed.

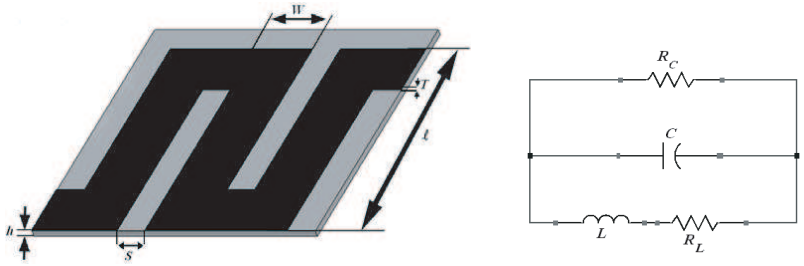

(a) (b)

Figure 1. Ungrounded meander line inductor, (a) geometrical parameters of a single turn ungrounded meander line inductor, (b) lumped element model of ungrounded meander line inductor.

The self inductance of meander line inductor is calculated based on Evaluation of Partial Inductances method which has been previously reported in [18, 19]. For calculation of the inductance of grounded meander line, each segment and its image should be taken into account. For rectangular segments, let the length be l and the widths of two sides be W and T, respectively. The self inductance for each segment of meander line inductor can be determined by (1) [19]. Defining the normalized width and thickness as $w = W/l$, $t = T/l$, and the normalized distances as follows

$$r = \left(w^2 + t^2\right)^{0.5}, \quad \alpha_w = \left(w^2 + 1\right)^{0.5},$$
$$\alpha_t = \left(t^2 + 1\right)^{0.5}, \quad \alpha_r = \left(w^2 + t^2 + 1\right)^{0.5}.$$

The self inductance of any segment can be written as follows

$$\frac{Ls}{\ell} = \frac{2\mu}{\pi}\left\{\begin{array}{l} 0.25\left[\frac{1}{w}S\left(\frac{w}{\alpha_t}\right) + \frac{1}{t}S\left(\frac{t}{\alpha_w}\right) + S\left(\frac{1}{r}\right)\right] \\ +\frac{1}{24}\left[\frac{t^2}{w}S\left(\frac{w}{t\alpha_t(r+\alpha_r)}\right) + \frac{w^2}{t}S\left(\frac{t}{w\alpha_w(r+\alpha_r)}\right) + \frac{t^2}{w^2}S\left(\frac{w^2}{tr(\alpha_t+\alpha_r)}\right)\right. \\ \left. + \frac{w^2}{t^2}S\left(\frac{t^2}{wr(\alpha_w+\alpha_r)}\right) + \frac{1}{wt^2}S\left(\frac{wt^2}{\alpha_t(\alpha_w+\alpha_r)}\right) + \frac{1}{tw^2}S\left(\frac{tw^2}{\alpha_w(\alpha_t+\alpha_r)}\right)\right] \\ -\frac{1}{6}\left[\frac{1}{wt}T\left(\frac{wt}{\alpha_r}\right) + \frac{t}{w}T\left(\frac{w}{t\alpha_r}\right) + \frac{w}{t}T\left(\frac{t}{w\alpha_r}\right)\right] \\ -\frac{1}{60}\left[\frac{(\alpha_r+r+t+\alpha_t)t^2}{(\alpha_r+r)(r+t)(t+\alpha_t)(\alpha_t+\alpha_r)} + \frac{(\alpha_r+r+w+\alpha_w)w^2}{(\alpha_r+r)(r+w)(w+\alpha_w)(\alpha_w+\alpha_r)}\right. \\ \left. + \frac{(\alpha_r+\alpha_w+1+\alpha_t)}{(\alpha_r+\alpha_w)(\alpha_w+1)(1+\alpha_t)(\alpha_t+\alpha_r)}\right] - \frac{1}{20}\left[\frac{1}{r+\alpha_r} + \frac{1}{\alpha_w+\alpha_r} + \frac{1}{\alpha_t+\alpha_r}\right] \end{array}\right\} \tag{1}$$

where $S(x) = \sinh^{-1}(x) = \ln x + (1 + x^2)^{0.5})$ and $T(x) = \tan^{-1}(x)$ denote the arc hyperbolic sine and tangent functions, respectively. The two main parameters of these inductors are the arm length l, separation between arms S and thickness of metallic layers T, that T is assumed to be constant ($T = 0.035\,\mathrm{mm}$). The partial mutual inductance depends mainly on the relative geometrical position and the lengths of the two segments and slightly on the shapes cross section. Considering two parallel segments of the same width W, thickness T, length l and centre-to-centre distance D ($D = S + W$). The mutual inductance between any two parallel segments can be achieved analytically by [20]

$$\mathrm{M} = \left[\frac{1}{2}(Ls_{D+T} + Ls_{D-T}) - Ls_D\right]\cdot\left(\frac{D}{T}\right)^2 + (Ls_{D+T} - Ls_{D-T})\cdot\left(\frac{D}{T}\right) + \frac{1}{2}(Ls_{D+T} - Ls_{D-T}) \tag{2}$$

where the self inductance (Ls) in (2) is determined by (1) with the subscript denoting the thickness of the segment, in which, W is width and l is length. Figure 2 shows the different forms of mutual differential segments for which mutual inductances are to be determined.

Total flux of grounded meander line inductor can be written as

$$\Phi = L \cdot I \tag{3}$$

where I denote the current of the meander line inductor and L is the equivalent inductance of a grounded meander line inductor that can be obtained as follows

$$L = Ls_{total} + |M_{total}| \tag{4}$$

In which, Ls_{total} and M_{total} are sum of self inductances and sum of mutual inductances, respectively. For calculating Ls_{total}, Eq. (1) should be applied to each segment and its image separately. In determination of M_{total}, mutual inductance between any two parallel arms is the most effective, especially in long arms, shown in Figure 2(c), which can be written as

$$M_{total} = \sum_{i=1}^{2N} (-1)^i \cdot 2 \cdot (2N - (i-1)) \cdot M(\ell, i \cdot s) \tag{5}$$

where M is obtained by (2) and N is the number of turns for a meander line inductor.

In (5) M_{total} may be calculated for $i = 1, 2$. Finally, Eq. (4) reduces to

$$L = Ls_{total} - M_1 + M_2 \tag{6}$$

where, M_1 and M_2 are sum of mutual inductances between any two adjacent arms and any two arms with $2S$ separation distance, respectively. The sign of mutual inductance is -1 or $+1$, depending on the currents directions. To show the validation of this approach, our results are compared with those previously reported results in [16]. It is assumed that the meander line inductor is mounted on a grounded substrate having thickness of ($h = 1.5\,\text{mm}$). Table 1 summarizes the results obtained by the proposed analytical method ($L_{analysed}$), including physical parameters (number of turns, l, W, and S) and the measurement results ($L_{measured}$) obtained from [16].

The mutual inductance between the l segments and their return path in the ground plane is neglected because of inversely current

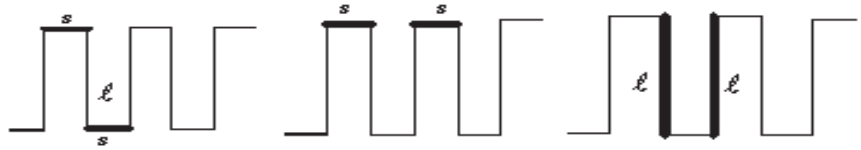

(a) (b) (c)

Figure 2. The forms of mutual segments.

Table 1. Analyzed and simulated inductance of the set of grounded meander-line inductors.

#	*Turns*	l (mm)	W (mm)	S (mm)	$L_{measured}$	$L_{analysed}$
1	4	10	0.4	0.4	34.2	30.228
2	2	10	0.6	0.4	16.1	13.421
3	4	10	0.6	0.4	27.6	26.229
4	2	10	0.8	0.4	14.3	12.271
5	4	10	0.8	0.4	25.3	24.069
6	2	10	1.0	0.4	13.8	11.490
7	4	10	1.0	0.4	22.6	22.535
8	2	10	2.0	0.4	9.89	9.2498
9	4	10	2.0	0.4	18.8	18.292
10	2	10	0.4	0.6	17.4	16.523
11	4	10	0.4	0.6	30.9	32.616
12	6	8	0.7	0.8	35.7	33.326
13	5	8	0.9	0.8	28.2	25.174
14	6	8	0.9	0.8	32.1	30.200
15	2	10	0.4	0.8	20.0	17.454
16	4	10	0.4	0.8	33.9	34.772
17	2	8	1.0	1.0	13.3	10.078
18	4	10	0.4	1.0	39.2	36.742
19	2	10	1.0	1.0	17.1	13.135
20	2	15	1.0	1.0	23.5	21.055
21	2	20	1.0	1.0	27.2	29.473
22	4	10	0.4	2.0	45.8	44.152

direction on two adjacent arms. As shown in Table 1, the results obtained by analytical method are agreed with the measured results. These results are valid at *VHF* and *UHF* bands depending on the physical parameters of meander line inductor. Finally, the ground plane may be removed and same the process can be applied again for the ungrounded meander line inductor.

Figure 3 shows the normalized input impedance of the ungrounded meander line inductor, Z_{in}, obtained by MoMs simulation, having resonant frequency beyond which the inductor acts as a capacitor, in other words, it can be modeled as a RLC parallel circuit. Input

impedance of meander line inductor can be determined by

$$Z = z_0 \frac{(1 + S_{11})}{(1 - S_{11})} \tag{7}$$

where, z_0 is $50\,\Omega$ reference impedance.

As shown in Figure 4, the ungrounded meander line inductor includes two types of capacitors. Conformal Mapping Method [21] can be applied for calculation of air gap capacitor and the dielectric gap capacitor is determined by [22] except for the removal of the ground plane. As the two adjacent parallel arms with reverse currents are similar to slot-line in odd mode, therefore, the following expression may be applied in slot-line odd mode for determination of C_{ga}

$$C_{ga} = \frac{\varepsilon_0 K(k')}{2K(k)} \tag{8}$$

where

$$k = S/(S + 2W), \quad k' = \sqrt{(1 - k^2)} \tag{9}$$

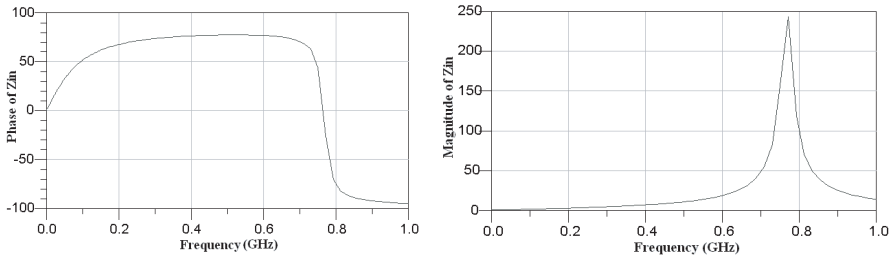

Figure 3. Ungrounded meander line inductor simulated at ADS momentum software, (a) phase of Z_{in}, (b) magnitude of normalized Z_{in}.

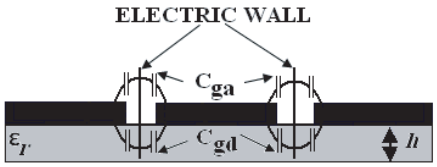

Figure 4. The capacitors of a single turn ungrounded meander line inductor in odd mode.

In which, W and S are the width of segment and distance between two adjacent arms, respectively. $K(k)$ and $K(k')$ denote the elliptic function and its complement. For determination of C_{gd}, one can write

$$C_{gd} = (\varepsilon_0 \varepsilon_{eff}/\pi) \cdot \ln(\coth(0.25\pi S/h)) \tag{10}$$

where

$$\varepsilon_{eff} = 0.5(\varepsilon_r + 1) \cdot \left(\tanh\left(1.785 \log\left(\frac{h}{W}\right) + 1.75\right)\right) + \left(k \cdot \frac{W}{h}\right) \cdot (0.04 - 0.7k + 0.01(1 - 0.1\varepsilon_r) \cdot (0.25 + k)) \tag{11}$$

Therefore, the gap capacitance of a single turn ungrounded meander line inductor, as shown in Figure 1(a), is determined by

$$C_g = (C_{ga} + C_{gd})/4 \tag{12}$$

And the total capacitance of N turns ungrounded meander inductor is obtained as

$$C = (N) \cdot (l) \cdot C_g \tag{13}$$

Table 2. Analyzed and simulated capacitance of the set of meander-line inductors.

#	***Turns***	***l*** **(mm)**	***W*** **(mm)**	***S*** **(mm)**	ε_r	***h*** **(mm)**	$C_{simulated}$ **(pF)**	$C_{analysed}$ **(pF)**
1	12	20	0.4	0.2	2.2	0.8	0.78761	0.72268
2	10	20	0.4	0.2	2.2	0.8	0.60223	0.72144
3	10	20	0.4	0.2	4.6	0.8	0.71901	0.85236
4	10	20	0.4	0.2	9.6	1.6	1.4178	1.1910
5	15	10	0.4	0.2	9.6	1.6	0.9949	0.89323
6	15	20	0.4	0.2	9.6	1.6	1.5135	1.7865
7	12	20	0.4	0.2	9.6	1.6	1.4610	1.4292
8	25	9	0.6	0.3	9.6	1.6	1.5096	1.1890
9	25	12	0.6	0.3	4.6	0.8	1.0548	0.9742
10	25	9	0.5	0.2	4.6	0.8	0.9686	0.8393
11	25	18	0.6	0.3	4.6	0.8	1.3379	1.4613
12	25	12	0.5	0.2	9.6	1.6	1.7396	1.8275
13	23	10	0.4	0.2	3.38	0.8	0.8156	0.7586
14	23	10	0.4	0.1	3.38	0.8	0.8135	0.9687
15	23	10	0.4	0.2	2.2	0.8	0.7863	0.6925

Finally, according to (6) and (13) resonant frequency of a ungrounded meander line inductor can be expressed as

$$f_{res_{MI}} = \frac{1}{2\pi\sqrt{LC}} \tag{14}$$

Table 2 shows the results obtained by proposed analytical method which agree with the simulation results obtained by ADS momentum software. More accurate equations may be obtained by considering other mutual inductances and by optimizing the effective ε_r.

2.2. Ungrounded Inter Digital Capacitor

Inter digital capacitors are widely used as passive elements in many microwave integrated circuits. Due to the simplicity of fabrication of the ungrounded inter digital capacitors on Coplanar Wave Guides (CPW); it is convenient to use these capacitors in periodic loading in planer transmission lines. The schematic diagram and the cross sectional view of ungrounded inter digital capacitor is shown in Figure 5, it consists of a set of inter digital fingers with geometrical parameters.

To obtain a closed form expressions for the capacitance of inter digital capacitor, Conformal Mapping method can be applied. The total capacitance, C of ungrounded inter digital capacitor is the sum of capacitances of each section, thus we need to calculate C_1, C_2 and C_3 shown in Figure 5(a) as follows [17]

$$C_1 = \varepsilon_0 \varepsilon_{eff_1} \frac{K(k_{01})}{K(k'_{01})} l \tag{15}$$

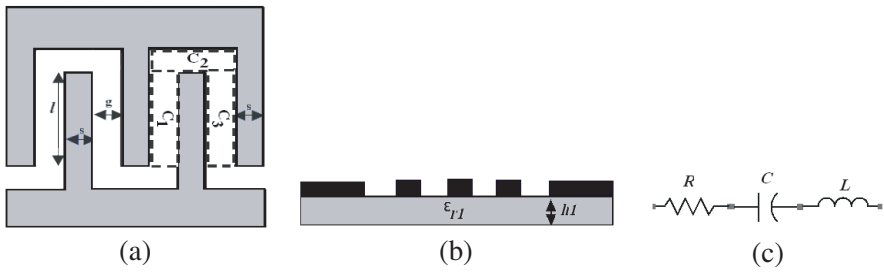

Figure 5. (a) Schematic of ungrounded inter digital capacitor, (b) cross-sectional view of ungrounded inter digital capacitor, (c) lumped element model of ungrounded inter digital capacitor.

where l is the length of the finger, $K(k_i)$ is the complete elliptic integral of the first kind, and

$$k_{01} = \sqrt{1 - \left(\frac{g}{g+s}\right)^2}, \quad \varepsilon_{eff_1} = 1 + q_1 \frac{\varepsilon_r - 1}{2} \tag{16}$$

$$q_1 = \frac{Kk_{11})}{K(k'_{11})} \frac{K(k'_{01})}{K(k_{01})}, \quad k_{11} = \sqrt{1 - \left(\frac{\sinh\left(\frac{\pi g}{4h}\right)}{\sinh\left(\frac{\pi(g+s)}{4h}\right)}\right)^2},$$
$$k'_{i1} = \left(1 - k_{i1}^2\right)^{0.5} \quad i = 0, 1 \tag{17}$$

The capacitance of the outer edge of section (C_3) is

$$C_3 = 4\varepsilon_0 \varepsilon_{eff2} \frac{K(k'_{02})}{K(k_{02})} l \tag{18}$$

where

$$k_{02} = \frac{s}{\sqrt{(g+s)(2g+s)}}, \ \varepsilon_{eff2} = 1 + q_2 \frac{\varepsilon_{r1} - 1}{2}, \ q_2 = \frac{K(k_{12})}{K(k'_{12})} \frac{K(k'_{02})}{K(k_{02})} \tag{19}$$

$$\begin{aligned} k_{12} = {} & [(\{\exp[\pi \cdot (3s + 2g)/h] - \exp[\pi \cdot (2g + s)/h]\} \\ & \times \{\exp(\pi s/h) - 1\})(\{\exp[\pi \cdot (3s + 2g)/h] \\ & - \exp(\pi s/h)\}\{\exp[\pi \cdot (2g + s)/h] - 1\})^{-1}]^{0.5}, \\ & k'_{i2} = \sqrt{(1 - k_{i2}^2)} \quad i = 0, 1 \end{aligned} \tag{20}$$

And the capacitance end section (C_2) of each finger can be obtained by

$$C_2 = 2\varepsilon_0 \varepsilon_{eff_1} \frac{K(k_{01})}{K(k'_{01})} L_{ext} \tag{21}$$

where

$$\begin{aligned} L_{ext} = {} & \frac{A}{12.5 \times 10^{-6}} \left[-4 \times 10^{-6} \left(\frac{s}{2A}\right)^2 + 9 \times 10^{-6} \left(\frac{s}{2A}\right) + 8 \times 10^{-6} \right] \\ & \times \left[1 + \left(\frac{A}{g + A}\right)^3 \right], \quad A = \frac{s + 2g}{4} \end{aligned} \tag{22}$$

where s as the width of fingers, g as the gap between two adjacent fingers, ε_r as the dielectric constant of substrate and h as the dielectric thickness are shown in Figure 5. Finally, the total capacitance of ungrounded inter digital capacitor with n fingers can be determined as follows

$$C = (n - 3)C_1 + C_2 + nC_3 \tag{23}$$

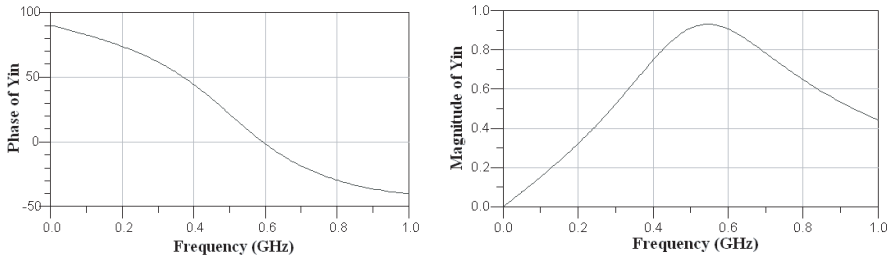

(a) (b)

Figure 6. Ungrounded inter digital capacitor simulated at ADS momentum software, (a) phase of Y_{in}, (b) magnitude of normalized Y_{in}.

As shown in Table 3, the results obtained by this analytical method agree with the measurement results [17]. Figure 6 shows normalized ungrounded inter digital capacitor Y_{in} having resonant frequency beyond which this capacitor behaves as an inductor, in other words, it is modeled as a RLC series circuit as shown in Figure 5(c). Input impedance of ungrounded inter digital capacitor can also be determined by (7).

Table 3. Analyzed and measured capacitance of the set of ungrounded inter-digital capacitors.

#	***Fingers number***	$C_{measured}$ **(pF)**	$C_{analysed}$ **(pF)**
1	10	0.09	0.089
2	20	0.16	0.186
3	50	0.5	0.477

The inductance of ungrounded inter digital capacitor can be calculated by the assumption that the small lateral gaps are approximately short-circuited. Then the inductance matrix $[L]$ can be expressed as follows

$$L_{IC} = \begin{pmatrix} L_{11} & L_{12} & \dots & L_{1(2n)} \\ L_{21} & L_{22} & \dots & L_{2(2n)} \\ \vdots & \vdots & \dots & \vdots \\ L_{(2n)1} & L_{(2n)2} & \dots & L_{(2n)(2n)} \end{pmatrix}_{2n \times 2n} \tag{24}$$

where L_{ii} is the self inductance of each finger obtained by (1), $L_{ij}(i \neq j)$ is the mutual inductance between any two fingers obtained by (2).

Inverse matrix of $[L_{IC}]([\Gamma])$ might be determined noting that capacitor fingers are parallel. The equal inductance can be obtained by

$$L = \frac{1}{\sum_{i=1}^{i=2n} \sum_{j=1}^{j=2n} \Gamma_{ij}} \tag{25}$$

where n is the number of capacitor fingers. Finally, according to (23) and (25) the resonant frequency of the ungrounded inter digital capacitor is obtained by

$$f_{res_{IC}} = \frac{1}{2\pi\sqrt{LC}} \tag{26}$$

As shown in Table 4 the results obtained by the proposed analytical method agree well with MoMs simulation results.

Table 4. Analyzed and simulated inductance of the set of ungrounded inter-digital capacitors.

#	*Fingers*	*l* (mm)	*W* (mm)	*S* (mm)	$L_{simulated}$ (nH)	$L_{analysed}$ (nH)
1	4	9.2	0.4	0.05	3.1102	2.2010
2	4	9.2	0.4	0.1	2.4471	2.1845
3	4	9.2	0.4	0.2	2.1046	2.1725
4	4	10	0.4	0.1	3.0194	2.4255
5	4	8	0.5	0.2	1.7942	1.7301
6	5	9.2	0.4	0.2	2.0092	2.1579
7	6	12	0.6	0.3	2.6814	2.7320
8	7	15	0.6	0.2	3.5441	3.5656
9	8	9.2	0.4	0.05	2.2239	2.1324
10	9	20	0.6	0.2	4.6078	4.9802
11	10	9.2	0.4	0.05	2.2560	2.0670
12	10	18	0.8	0.3	2.5695	2.6027
13	10	20	0.8	0.3	3.1892	3.7564
14	12	20	0.6	0.2	3.2307	2.9981
15	5	25	0.5	0.2	6.7796	6.9278

3. ANALAYZING AND DESIGN OF ANTENNA

A CRLH cell and its equivalent circuit model are shown in Figure 7, which is periodically loaded on the antenna. Figure 8 shows the unloaded dipole antenna and CRLH loaded dipole antenna

configurations. Radiation mechanism of this antenna has been studied in [11], when a voltage is applied at the feed point, the currents I_1 and I_2, shown in Figure 8, have different amplitude levels and are out-of-phase. As distance d is much smaller than a free space wavelength, λ_0, phase difference in the two paths will not affect the far field radiation of the currents I_1 and I_2 in which case, the radiation source becomes the summation of I_1 and I_2.

As the currents in the x direction are out-of-phase at the symmetrical positions for the feed point, cross polarization remains in a low level. The interesting feature of the CRLH loaded dipole antenna is the excitation of negative resonance modes of dipole antenna at lower frequencies. In addition to the fundamental resonance mode of $m = -1$, higher order negative resonance modes will be excited, even if the CRLH loaded antenna length is less than the free space wavelength, λ_0. Based on the characteristics of an ideal homogenous balanced CRLH resonator, we have [15]

$$\ell = |m| \frac{\lambda}{2}, \quad \beta_m = \left(\frac{2\pi}{\lambda}\right) \tag{27}$$

where, ℓ is length of dipole antenna, the number m is a negative integer, and λ is induced current wavelength, which is controlled by inductors and capacitors. Dispersion relation can be expressed for the dipole antenna loaded with CRLH structures, also operating in negative resonances. In other words, this dipole antenna will have $0.5\lambda_u$ length, wherein λ_u is unloaded dipole antenna wavelength, even in lower frequencies, resulting in the miniaturization of printed dipole antenna. Resonance frequencies of this antenna in negative mode numbers can be determined analytically versus unloaded dipole antenna resonance frequency f_{un}, C_R, C_L, L_R, L_L. Based on phase constant β related to an infinite transmission line loaded with the CRLH cells, and is expressed as [15]

$$\beta = \frac{1}{p} \times \cos^{-1}\left\{1 - \frac{1}{2}\left[\frac{1}{\omega^2 L_L C_L} + \omega^2 L_R C_R - \left(\frac{L_R}{L_L} + \frac{C_R}{C_L}\right)\right]\right\} \tag{28}$$

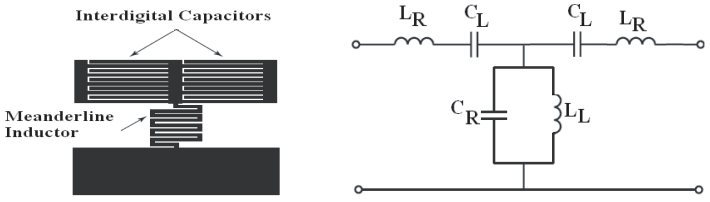

Figure 7. (a) A CRLH cell, (b) the equal circuit model of CRLH cell.

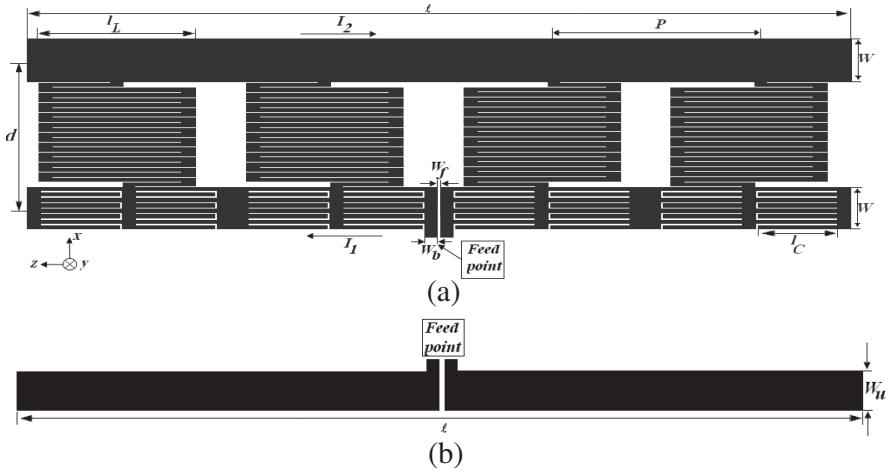

Figure 8. The schematics and design parameters of (a) the dipole antenna loaded with CRLH structures, (b) unloaded dipole antenna.

where ω is angular frequency, p is periodic distance between two subsequent cells. Let N be the number of CRLH cells loaded on antenna and ℓ the length of dipole antenna. First, by means of Eqs. (27) and (28), constant values, A and B, can be defined as follows

$$A = \frac{2\pi \cdot p \cdot m. \cdot f_{ru} \cdot \sqrt{\varepsilon_{eff}}}{C} \quad m < 0,$$
$$B = 2(1 - \cos(|A|)) + \left(\frac{L_R}{L_L} + \frac{C_R}{C_L}\right) \tag{29}$$

where f_{ru} is resonance frequency of the unloaded printed dipole antenna in free space, C the velocity of light in free space and ε_{eff} the effective dielectric constant for narrow trace [23], and assumed $W_u = 0.05h$ as shown in Figure 8(b). Then, according to (28) and (29), resonance frequency in negative mode is obtained as follows

$$b_1\omega_m^4 - b_2\omega_m^2 + 1 = 0,\ b_1 = L_R L_L C_R C_L,\ b_2 = BL_L C_L,\ f_m = \omega_m/2\pi \tag{30}$$

where L_R and C_L are related to ungrounded inter digital capacitor, L_L and C_R are related to ungrounded meander line inductor. Eq. (30) has four roots that one of them is acceptable which shows the resonance frequency of negative mode number. For clarity, the results obtained by this analytical method are compared with HFSS simulation results in Table 6. According to Figure 8, constant parameters of simulated antennas in Table 6 are mentioned in Table 5.

Table 5. Parameters of the simulated and fabricated dipole antenna shown in Figure 8(a).

Length L of the antenna	100 mm
Periodic distance p	25 mm
Distance d of lines	16.6 mm
Width W of lines	4.6 mm
Number N of CRLH cells	4
Ungrounded inter digital capacitor length l_C	9.2 mm
Ungrounded meander line inductor length l_L	23 mm
Unload printed dipole antenna resonance frequency in free space f_{ru}	1.5 GHz
Width of slot W_f	0.2 mm
Width of matched balun slot-line W_b	1.8 mm

Table 6. A comparison between analytical and simulated results for $m = -1$.

#	ε_r	h (mm)	g_{ic} (mm)	g_{mi} (mm)	L_R (nH)	C_L (pF)	L_L (nH)	C_R (pF)	$fr_{analysed}$ (GHz)	$fr_{simulated}$ (GHz)
1	3.38	0.8	0.1	0.1	2.1845	3.9392	63.545	0.96879	0.2518	0.252
2	3.3	0.8	0.1	0.2	2.1845	3.8686	71.733	0.75412	0.262	0.268
3	**2.2**	**0.8**	**0.2**	**0.2**	**2.1725**	**3.2767**	**71.733**	**0.6926**	**0.298**	**0.275**
4	3.55	0.8	0.2	0.2	2.1725	4.3014	71.733	0.76811	0.234	0.235

4. SIMULATION AND MEASUREMENT RESULTS

Figure 9 shows the fabricated printed dipole antenna loaded with CRLH structures. The antenna is implemented on Taconic substrate with thickness of 0.8 mm, permittivity of 2.2 and loss tangent of 0.0009 that its CRLH parameters are highlighted in Table 6. The parameters of simulated and fabricated antenna shown in Figure 8 are mentioned in Table 5. The antenna is simulated in HFSS environment. The widths of lines and gaps are 0.4 mm and 0.2 mm respectively for ungrounded meander line inductor and ungrounded inter digital capacitor. The number of digits of ungrounded inter digital capacitor is 4 and the number of the turns of ungrounded meander line inductor is 10. The

balun as shown in Figure 9(b), is composed of four sections to convert the balanced electrical field, TEM mode of coaxial feeding line, to unbalanced slot-line electrical field [24].

Figure 10 shows the reflection characteristic of the simulated antenna through the balun with inter digital capacitor gap 0.1 mm on Rogers RO4003 substrate with permittivity 3.38 and analytical resonant frequencies on simulation curve have been determined for $m = -1$ and $m = -3$. As shown in Figure 10(a), resonance modes of $m = 1$, $m = 0$, $m = -1$, $m = -3$ and $m = -5$ are appeared. Inter digital capacitor gap is increased to 0.2 mm with Taconic substrate because of fabrication limitations. HFSS simulation and the measured reflection characteristic are shown in Figure 10(b), in measured one, not only fundamental mode $m = -1$ at 326.0 MHz but also two higher order modes $m = -3$ at 244.6 MHz and $m = -5$ at 231.3 MHz are appeared.

As shown in Figure 10(b), frequency shift Δf, between simulation and measurement results is 51 MHz for $m = -1$. HFSS simulation inaccuracy in structures with such small gaps and manufacturing tolerance in antenna realization such as those related to physical dimensions of substrate and substrate permittivity tolerances at low frequencies are responsible for Δf. In other words, the dielectric substrate is modified in the different frequencies i.e., the antenna performance is modified and as a result, the values of the capacitors and inductors have to be adjusted so that the resonant frequency would be nearly the same as that of obtained by analytical method and input impedance would be matched with feed line. An input impedance with a real part close to 50 Ω and a imagine part is nearly zero, is achieved at 326.0 MHz in $m = -1$ mode and bandwidth is 3%. Length of the antenna for $m = -1$ resonance mode, is $0.1\,\lambda_0$ wherein, λ_0 is free space wavelength. It should be also pointed out that the relationship between negative resonance modes and their corresponding frequencies is nonlinear.

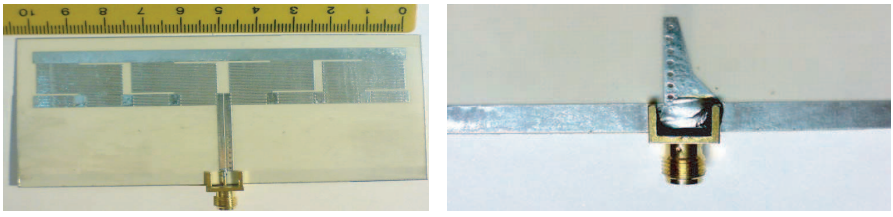

(a) (b)

Figure 9. (a) Photograph of the printed CRLH loaded dipole antenna with its balun, (b) balun configuration on the back of the substrate.

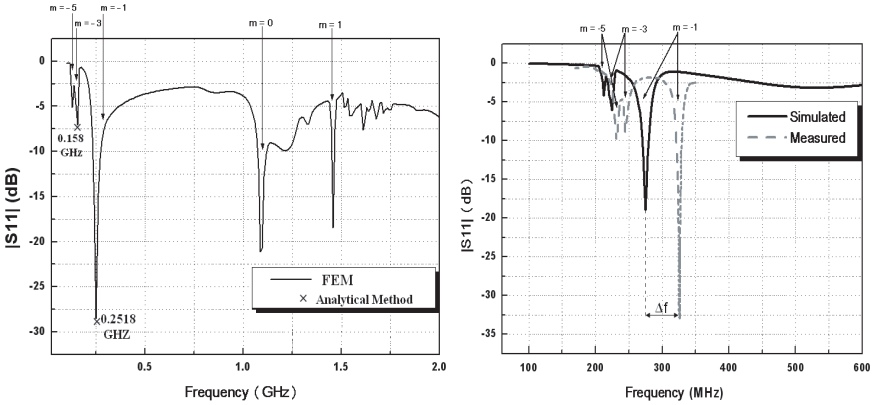

Figure 10. Reflection characteristic of the CRLH loaded printed dipole antenna through the balun (a) with inter digital gap = 0.1 mm and $\varepsilon_r = 3.38$ (—: FEM, ×: analytical method), (b) with inter digital gap = 0.2 mm and $\varepsilon_r = 2.2$. (—: Mea., - - -: FEM).

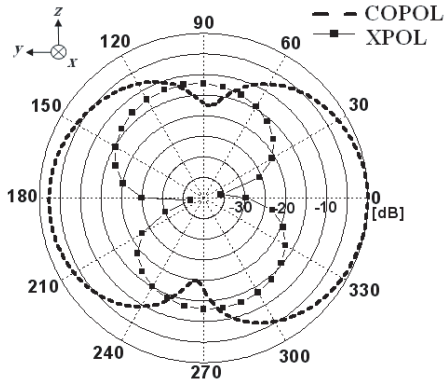

Figure 11. Measured E-plane normalized radiation pattern of the CRLH loaded printed dipole antenna in yz plane at 326.0 MHz, $m = -1$.

The radiation pattern is measured in the yz plane at 326.0 MHz and is shown in Figure 11. The radiation pattern is obtained as expected from a dipole antenna. Measured gain is −8.9 dB and the loss of the balun is less than 0.5 dB which is included in the gain value. Cross polarization is lower than −12 dB in case of $m = -1$ mode.

5. CONCLUSION

An analytical modeling to characterize the frequency behavior of a printed dipole antenna loaded with the CRLH structures is presented. The CRLH loading is realized by means of ungrounded inter digital capacitors as series and ungrounded meander line inductors as shunt components. A governing formula for obtaining the resonant frequencies in negative resonance modes related to the CRLH loaded antenna by means of dispersion relation and versus the parameters of ungrounded inter digital capacitors, ungrounded meander line inductors and the unloaded dipole antenna resonance frequency is proposed. Also, the essential expressions of the parameters of ungrounded inter digital capacitor and ungrounded meander line inductor in low frequencies, UHF band for a computer implementation, are proposed. For calculation of capacitance of the CRLH structures, conformal mapping method is used. Advantages of the proposed analytical method are that it gives us the liberty to manage the antenna miniaturization at fundamental negative mode frequency, in addition, CRLH structures parameters are determined by proposed closed form expressions. Length of the CRLH loaded dipole antenna is much shorter than $0.5\,\lambda_0$ for $m = -1$ resonance mode, that is $0.1\,\lambda_0$. The main challenge of CRLH loaded dipole antennas is the optimization of efficiency.

The short length of the CRLH loaded printed dipole antenna, makes it suitable for small antenna applications. In other words, loading the CRLH structures on the antennas is a novel approach for antenna miniaturization. It is clear that the concept of the CRLH structures and their applications with regard to antennas, are significantly increasing, making antennas suitable for different applications.

ACKNOWLEDGMENT

The authors would like to thank Iran Telecommunication Research Center (ITRC) for its financial supports.

REFERENCES

1. Caloz, C. and T. Itoh, "Transmission line approach of left-handed (LH) materials and microstrip implementation of an artificial LH transmission line," *IEEE Tans. Antenna Propagat.*, Vol. 52, No. 5, 1159–1166, May 2004.

2. Caloz, C., A. Sanda, and T. Itoh, "A novel composite right-/left-handed coupled-line directional coupler with arbitrary coupling level and broad bandwidth," *IEEE Tans. Microwave Theory Tech.*, Vol. 52, 980–992, Mar. 2004.
3. Gil, M., J. Bonache, J. Selga, J. Garcia-Garcia, and F. Martin, "High-pass filters implemented by composite right/left handed (CRLH) transmission lines based on complementary split rings resonators (CSRRs)," *PIERS Online*, Vol. 3, No. 3, 251–253, 2007.
4. Sebak, S., L. Zhu, V. K. Devabhaktuni, and C. Wang, "A CRLH microstrip delay line for high-speed electronic circuits," *PIERS Online*, Vol. 3, No. 3, 259–263, 2007.
5. Jimenez-Martin, J. L., V. Gonzialez-Posadas, J. E. Gonzalez-Garcia, F. J. Arques-Orobon, L. E. Garcia Munoz, and D. Segovia-Vargas "Dual band high efficiency class CE power amplifier based on CRLH diplexer," *Progress In Electromagnetics Research*, PIER 97, 217–240, 2009.
6. Liu, L., C. Caloz, and T. Itoh, "Dominant mode leaky-wave antenna with backfire-to-endfire scanning capability," *Electron. Lett.*, Vol. 38, No. 23, 1414–1416, Nov. 2002.
7. Schuessler, M., J. Freese, and R. Jakoby, "Design of compact planar antennas using LH-transmission lines," *Proc. IEEE Int. Symp. Microwave Theory and Tech.*, Vol. 1, 209–212, Jun. 2004.
8. Qureshi, F., M. A. Antoniades, and G. V. Eleftheriades, "A compact and low-profile metamaterial ring antenna with vertical polarization," *IEEE Antennas Propagat. Lett.*, Vol. 4, 333–336, 2005.
9. Ziolkowski, R. W. and A. D. Kipple, "Application of double negative materials to increase the power radiated by electrically small antennas," *IEEE Trans. Antennas Propagat.*, Vol. 51, No. 10, 2626–2640, Oct. 2003.
10. Iizuka, H. and P. S. Hall, "A left-handed dipole concept," *Proc. Int. Workshop on Antenna Tech.*, New York, Mar. 6–8, 2006.
11. Iizuka, H. and P. S. Hall, "A left-handed dipole antenna and their implementations," *IEEE Trans. Antennas Propagat.*, Vol. 55, No. 5, May 2007.
12. Liu, Q., P. S. Hall, and A. L. Borja, "Dipole with left handed loading with optimized efficiency," *2nd European Conference on Antenna and Propagation, EUCAP07*, Edinburgh, Nov. 2007.
13. Niu, J.-X. and X.-L. Zhou, "Analysis of balanced composite right/left handed structure based on different dimensions of complementary split ring resonators," *Progress In Electromagnetics*

Research, PIER 74, 341–351, 2007.

14. Sanchez-Martinez, J. J., E. Marquez-Segura, P. Otero, and C. Camacho-Penalosa, "Artificial transmission line with left/right-handed behavior based on wire bonded interdigital capacitors," *Progress In Electromagnetics Research B*, Vol. 11, 245–264, 2009.
15. Caloz, C. and T. Itoh, *Electromagnetic Metamaterials: Transmissiion Line Theory and Microwave Applications*, Wiley-Intersience, Hoboken, NJ, 2006.
16. Acuna, J. E., J. L. Rodriguez, and F. Obelliero, "Design of meander line inductors on printed circuit boards," *Int. J RF and Microwave*, John Wiley & Sons, Feb. 2001.
17. Yoon, H., K. J. Vinoy, and V. K. Varadan, "Design and development of micromachined bilateral interdigital coplanar waveguide RF phase shifter compatible with lateral double diffused metal oxide semiconductor voltage controlled on silicon," *Institute of Physics Publishing*, Sep. 2003.
18. Ruehli, A. E., "Inductance calculations in a complex integrated circuit environment," *IBM J. Res. Develop.*, 470–481, 1972.
19. Wu, R. B., C. N. Kuo, and K. K. Chang, "Inductance and resistance computations for three-dimensional multiconductor interconnection structures," *IEEE Tans. Microwave Theory Tech.*, Vol. 40, No. 2, 263–271, Feb. 1992.
20. Grover, F. W., *Inductance Calculations: Working Formulas and Tables*, Van Nostrand, New York, 1992.
21. Collin, R. E., *Foundations for Microwave Engineering*, Wiley-Intersience, Hoboken, NJ, 1992.
22. Gupta, K. C., R. garg, and I. J. Bahl, *Microstrip Lines and SlotLines*, Artech House, Washington, 1979.
23. Johnson, H. W. and M. Graham, *High Speed Digital Design*, Prentice Hall PTR, April 1993.
24. Kim, Y. G., D. S. Woo, K. W. Kim, and Y. K. Cho, "A new ultra-wideband microstrip-to-CPS transition," *IEEE MTT-S International Microwave Symposium*, Daegu, Korea, Jun. 2007.